



Contents lists available at ScienceDirect

# Spectrochimica Acta Part A: Molecular and Biomolecular Spectroscopy

journal homepage: [www.elsevier.com/locate/saa](http://www.elsevier.com/locate/saa)

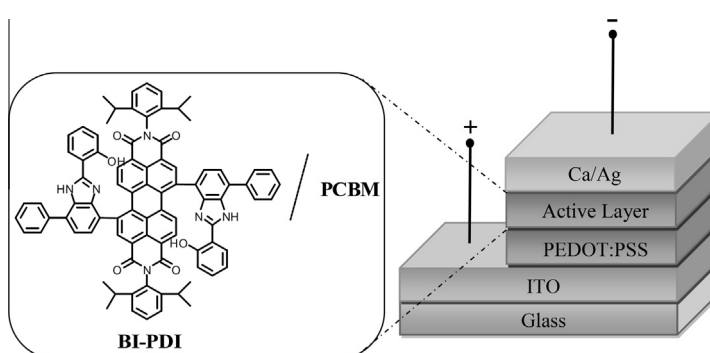
## Synthesis, characterization and optoelectronic properties of a new perylene diimide–benzimidazole type solar light harvesting dye

Haluk Dinçalp<sup>a,\*</sup>, Oguzhan Çimen<sup>a</sup>, Tayebah Ameri<sup>b</sup>, Christoph J. Brabec<sup>b</sup>, Siddik İçli<sup>c,\*</sup><sup>a</sup> Department of Chemistry, Faculty of Arts and Science, Celal Bayar University, Muradiye, 45030 Manisa, Turkey<sup>b</sup> Institute of Materials for Electronics and Energy Technology (I-MEET), Friedrich-Alexander-University, Martensstraße 7, 91058 Erlangen, Germany<sup>c</sup> Solar Energy Institute, Ege University, Bornova, 35100 Izmir, Turkey

### HIGHLIGHTS

- Benzimidazole-substituted PDI dye for solution-processed BHJc was synthesized.
- Aggregation tendency of dye in the presence of P3HT polymer was observed.
- Electron mobility of PDI dye is calculated to be higher than the hole mobility.

### GRAPHICAL ABSTRACT



### ARTICLE INFO

#### Article history:

Received 22 December 2013  
 Received in revised form 31 January 2014  
 Accepted 19 February 2014  
 Available online 10 March 2014

#### Keywords:

Perylene diimide  
 Benzimidazole  
 Photoluminescence  
 Charge transfer  
 Light harvesting  
 Photovoltaics

### ABSTRACT

A perylene diimide type small molecule (**BI-PDI**) has been synthesized through Suzuki coupling reaction between *N,N'*-bis(2,6-diisopropylphenyl)-1,7-dibromoperylene-3,4,9,10-tetracarboxylic diimide and 2-(2-hydroxyphenyl)-7-phenyl-1H-benzimidazole-4-boronic acid. **BI-PDI** small molecule has showed an absorption band between 350 and 750 nm on thin films. HOMO and LUMO energy levels of **BI-PDI** dye have been calculated to be about  $-5.92$  eV and  $-3.82$  eV, respectively. Solution-processed bulk heterojunction (BHJ) solar cells have been constructed using **BI-PDI** as donor and [6,6]-phenyl-C<sub>61</sub>-butyric acid methyl ester (PC<sub>61</sub>BM) as acceptor or poly(3-hexylthiophene) (P3HT) as donor and **BI-PDI** as acceptor. The external quantum efficiencies (EQE) of the devices cover the most of the visible region between 400 and 700 nm for both configurations. Photovoltaic performances of **BI-PDI**-based organic solar cells are limited by the aggregation tendency of PDI structure and poor hole/electron mobilities of the active layer.

© 2014 Elsevier B.V. All rights reserved.

### Introduction

Small molecule semiconductors have been extensively used in BHJ solar cells for decades due to their exclusively properties such

as well-ordered molecular structures, simple synthetic pathways, well-defined molecular weights, easily changeable spectral tunings by variation of functional groups and advantageous on thin film morphology [1,2]. Nowadays most of the organic photovoltaic (OPV) materials have been configured by using well-known conjugated small molecules including phthalocyanines [3,4], boron-dipyrromethenes [5,6], fused acenes [7–9], thiazoles [10,11], triphenylamines [12,13], diketopyrrolopyrroles [14,15], isoindigos [16], tetraphenylphthalic-based diimides [17], and fullerenes

\* Corresponding authors. Tel.: +90 236 2013158; fax: +90 236 2412158 (H. Dinçalp). Tel./fax: +90 232 3740118 (S. İçli).

E-mail addresses: [haluk.dincalp@cbu.edu.tr](mailto:haluk.dincalp@cbu.edu.tr) (H. Dinçalp), [siddik.icli@ege.edu.tr](mailto:siddik.icli@ege.edu.tr) (S. İçli).

[18]. However, they have had still lower power conversion efficiencies (PCEs) with respect to their polymeric counterparts. It will be expected that higher efficiencies can be obtained by the development of suitable molecular designs for small molecule organic semiconductors in near future studies. Among the preferred small molecule-based BHJ configurations, donor–acceptor networks containing perylene diimides (PDIs) as acceptors and appropriate donor materials lead to efficient photoinduced charge separation in OPVs [19–21].

PDIs are suitable candidates as an acceptor in device structures due to their stronger visible absorptions within the range of 400–450 nm (B band) and 500–700 nm (Q band), better charge transporting properties [22], higher molar absorption coefficients [23], higher fluorescence quantum yields [24] and better photostabilities [25] under solar irradiation as compared to their conjugated counterparts. In the literature survey, PCE values given for OPV devices using PDI small molecules as acceptor are found within the wide range of 0.002–3.17 depending on both the nature of the active layer and the used techniques [26–33]. Sharma et al. have blended 1,7-substituted perylene-anthracene diimide with a donor molecule containing dithienyl-benzothiadiazole central unit and obtained PCE of 2.85% with short-circuit current density of 6.8 mA/cm<sup>2</sup> [27]. A diphenoxylated PDI small molecule in bay positions of perylene ring has been used as acceptor and *p*-phenylene-vinylene type small group has been used as donor group in OPV device with ZnO layer giving PCE of 3.17% by Sharma et al. in different study [33]. In that device, the PCE has been improved by both incorporating ZnO layer between the active layer and the Al electrode and also annealing to increase the crystalline of the active layer. Han et al. have manufactured the ternary structure for OPV device consisting of P3HT:PCBM with the addition of a butoxyphenoxy substituted PDI molecule and obtained a considerable improvement of over 70% in PCE with respect to reference cell without an additive [34].

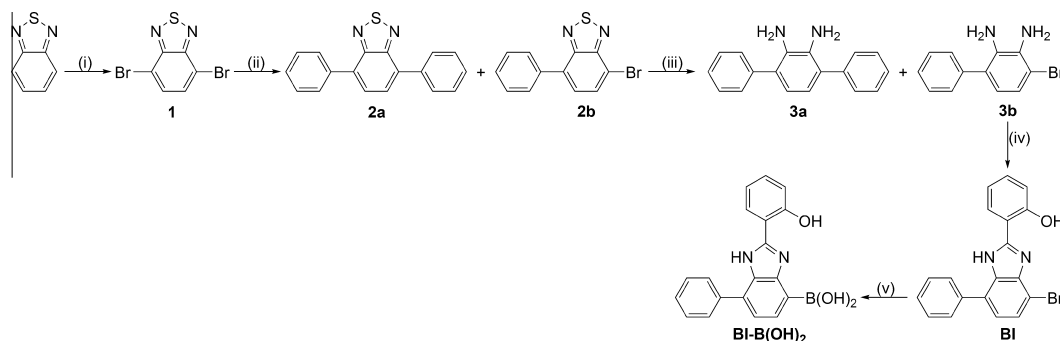
Generally, PDIs show two reduction waves with their planar structure responsible for high degree of  $\pi$ – $\pi$  stacking [35–37]. The introduction of bulky substituents in bay positions of the ring disturbs the planarity of the perylene core. These deviations from planarity may decrease multi-dimensional electron transfer processes. Also, deformations from molecular planarity results the inhibition of aggregation which may be helpful to improve PCE of a desirable device. In such efforts, bay-functionalized groups on the perylene ring are the most important molecular building blocks for an effective OPV device [38]. The report herein is based to decrease the molecular planarity of perylene core by attaching with special benzimidazole derivative in 1- and 7-positions of the perylene ring. There are a limited number of studies about small organic molecules based on benzimidazole for OPV devices in the literature. A recent study is related to 2,2-dimethyl-2H-benzimidazole small molecule-based BHJ solar cell comprising benzimidazole derivative with PC<sub>61</sub>BM giving FF of 27 with a low PCE of 0.37 [39].

In present work, we also targeted to synthesize a low band gap material by incorporating benzimidazole group to the perylene core. This kind of benzimidazole substituted PDI-type small molecule (**BI-PDI**) may ascribe the intramolecular charge generation. The absorption and emission properties of the dye in common solvents of different polarities and also on thin films have been investigated in detail. Also, hole and electron mobility performances of some selected devices have been tested. Synthetic routes and dye structures are shown in Schemes 1 and 2.

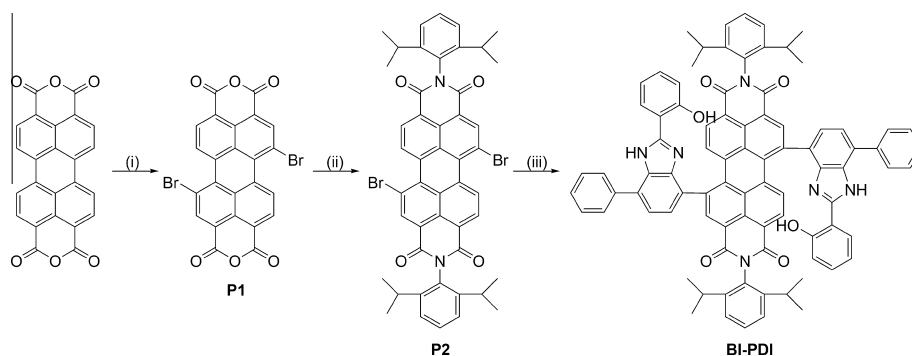
## Experimental

### General procedures

<sup>1</sup>H NMR and <sup>13</sup>C NMR spectra for characterization of the synthesized compounds were recorded on a Bruker 400 MHz



**Scheme 1.** Reaction pathway for the synthesis of **BI-B(OH)<sub>2</sub>**. (i) Br<sub>2</sub>/HBr, 120 °C, 93% [40]; (ii) phenylboronic acid, Na<sub>2</sub>CO<sub>3</sub>, benzene, Pd(PPh<sub>3</sub>)<sub>4</sub>, 80 °C, 10% (for **2b**) [41]; (iii) EtOH/THF, NaBH<sub>4</sub>, CoCl<sub>2</sub>·6H<sub>2</sub>O, 80 °C [42]; (iv) Salicyl aldehyde, Me-CN, CoCl<sub>2</sub>·6H<sub>2</sub>O, room temp., 95% [43]; (v) *n*-BuLi, THF, –78 °C, B(OMe)<sub>3</sub>, 75% [44].



**Scheme 2.** Reaction pathway for the synthesis of target **BI-PDI**. (i) H<sub>2</sub>SO<sub>4</sub>/Oleum, Br<sub>2</sub>, 85 °C, 84% [45]; (ii) 2,6-diisopropylaniline, propionic acid, 130 °C, 72% [45]; (iii) 2-(2-hydroxyphenyl)-7-phenyl-1H-benzimidazole-4-boronic acid, **BI-B(OH)<sub>2</sub>**, Na<sub>2</sub>CO<sub>3</sub>, Ar, Pd(OAc)<sub>2</sub>, 80 °C, 80% [35].

spectrometer. FT-IR spectra (KBr pellets) were recorded on a Perkin Elmer-Spectrum BX spectrophotometer. UV-visible spectra were measured on a Perkin Elmer Lambda 950 UV/VIS/NIR spectrophotometer in the solutions and on thin films. Fluorescence measurements were performed on a FLSP 920 Edinburg fluorescence phosphorescence spectrophotometer.

The fluorescence decays of the dye in solutions were occupied with laser system. The Edinburgh Instruments F900 reconvolution software based on the Marquardt Levenberg algorithm [46] was utilized for calculations. Up to 4 lifetimes could be fitted from up to 10,000 data channels with iterative shift fit, background fit and parameter fixing options. The fitted decay curve, together with lifetime and amplitude values, weighted residuals,  $\chi^2 < 1.2$  goodness of fit, autocorrelation function, etc. were all calculated to allow an assessment of the quality of the fit. The instrument response function (IRF) was measured using a ludox scattering solution. Solutions of the samples were contained in 1 cm path-length quartz cells at the optical density between 0.10 and 0.18 for fluorescence studies.

The cyclic voltammetry was performed on a CH instruments (Electrochemical Workstation) with a standard three-electrode electrochemical compartment in 100 mM [TBA][PF6] solution in Me-CN in room temperature under nitrogen purge. Ag/Ag<sup>+</sup> reference electrode, a glassy carbon working electrode and a Pt wire counter electrode were used. The scanning rate was 50 mV/s. Ferrocene-ferrocenium (Fe/Fe<sup>+</sup>) couple which was exhibited at about +0.55 V was used as internal reference for the calculation of the onset values of  $E_{\text{red}}$ . Redox potentials of BI-PDI were calculated from reversible waves with the formula  $[E_{\text{p(ox)}} + E_{\text{p(red)}}]/2$ .

#### Device preparation and testing

All the organic solar cells were constructed on indium tin oxide (ITO)-covered glass substrates (2.5 × 2.5 cm) as a normal structure configuration. First of all, the substrates were cleaned in an ultrasonic bath of isopropanol and acetone, respectively prior to device preparation. Poly(3,4-ethylenedioxy thiophene)/poly(styrene sulfonic acid) (PEDOT:PSS) was coated by a doctor-blade technique at a substrate temperature of 50 °C. PC<sub>61</sub>BM and other photoactive components were dissolved at concentrations of 2 wt% from *o*-dichlorobenzene (*o*DCB) solution in different mass ratios. Active layers consist of different configurations such as BI-PDI:PC<sub>61</sub>BM, P3HT:BI-PDI or BI:PC<sub>61</sub>BM structures and deposited with a typical film thickness of around 80–100 nm, which was measured by profilometer. Films were then annealed at 65 °C for 10 min under air. The Ca/Ag (15 nm/80 nm) metal electrode was thermally deposited. All the devices were constructed in air and then stored in glove box.

Solar cells were illuminated under AM1.5G irradiation on an OrielSol 1A Xenon solar simulator (100 mW cm<sup>-2</sup>). The current-voltage characteristics were measured using a Keithley 2400 SMU under nitrogen atmosphere. The surface of the thin films was investigated by Ambios Qscope 250 Model Atomic Force Microscope. Thicknesses of the active layers of the thin films were measured by Ambios Q1 Profilometry instrument. The EQE was detected with a lock-in amplifier (SR830, Stanford Research Systems) with current preamplifier (HMS-74) under monochromatic illumination, which was calibrated with a mono-crystalline silicon diode.

We fabricated the hole and electron only devices with the structures ITO/PEDOT:PSS/Active Layer/PEDOT:PSS/Ag(100 nm) and ITO/AZO(HT)/Active Layer/Ca(15 nm)/Ag(80 nm), respectively. Aluminum-doped zinc oxide (AZO) nanoparticles at high temperature were used in electron only device fabrication. These devices were prepared by the same way as organic solar cell production. We estimated the electron and hole mobilities according to the equation [33]:

$$J_{\text{SCL}} = \frac{9}{8} \epsilon_0 \epsilon_r \mu \frac{V_{\text{in}}^n}{L^3} \exp\left(\frac{0.89 \times \beta}{\sqrt{L}} \sqrt{V}\right)$$

where  $J$  was the current density,  $V$  was applied voltage,  $\epsilon_r$  (2.7 for blends) and  $\epsilon_0$  were the relative dielectric constants of the organic layer and permittivity of free space ( $8.85 \times 10^{-12}$  As/Vm), respectively,  $\mu$  was the electron mobility and  $L$  (100 nm) was the thickness of the organic layer.

#### Materials

1,7-Dibromo-perylene-3,4,9,10-tetracarboxylic dianhydride (**P1**) and N,N'-bis(2,6-diisopropylphenyl)-1,7-dibromoperylene-3,4,9,10-tetracarboxylicdiimide (**P2**) were synthesized according to the well-known procedure as shown in Scheme 2. Phenyl boronic acid was synthesized according to the standard procedure given in the literature [44]. 2,1,3-benzothiadiazole, NaBH<sub>4</sub>, Tetrakis(triphenylphosphine)palladium(0) Pd(PPh<sub>3</sub>)<sub>4</sub>, palladium acetate, salicyl aldehyde, bromobenzene, *n*-butyllithium (1.6 M in hexane), hydrochloric acid were purchased from Sigma Adrich. Trimethyl borate, perylene-3,4,9,10-tetracarboxylic acid dianhydride, propionic acid, cobalt(II) chloride hexahydrate and bromine were purchased from Merck company. 2,6-Diisopropylaniline (Acros Organics) and hydrogen bromide (Riedel-de Haen) were used as received. Other chemical reagents and organic solvents were analytical grade and used without further purification.

ITO coated glass with a surface resistance lower than 20 Ω/sq (Osram) was used as transparent electrode. PEDOT:PSS was obtained from Baytron PH H.C. Starck and P3HT was supplied from Rieke Inc. for the device preparation. Technical grade PCBM was purchased from Solenne.

#### Synthesis

##### Synthesis of 4,7-dibromo-2,1,3-benzothiadiazole (**1**)

2,1,3-Benzothiadiazole (3 g, 22.0 mmol) was dissolved in 65 mL of HBr (47%). On the other hand, Br<sub>2</sub> (3.5 mL, 68.3 mmol) was diluted with 45 mL of HBr. A solution containing Br<sub>2</sub> was added dropwise to the 2,1,3-benzothiadiazole solution. Then, extra 30 mL of HBr was added to the solution and the solution was stirred at 120 °C under an argon atmosphere for 15 h. Then, the mixture was cooled to room temperature and a sufficient amount of saturated solution of NaHSO<sub>3</sub> was added to the solution to remove the excess Br<sub>2</sub> completely. The solution was filtered off and then washed with Et<sub>2</sub>O. The yellow solid was purified by column chromatography on silica gel using dichloromethane:*n*-hexane (3:2) as an eluent. Yield: 93%, FT-IR (KBr pellet, cm<sup>-1</sup>): 3078, 3045, 1574, 1498, 1476, 1310, 1273, 1184, 937, 875, 826, 587, 488 cm<sup>-1</sup>. <sup>1</sup>H NMR (400 MHz, DMSO-d<sub>6</sub> δ 2.48 ppm): δ = 7.92 (s) ppm. <sup>13</sup>C NMR [100 MHz, DMSO-d<sub>6</sub> δ 40.2 ppm (7 peaks)]: δ = 162.9, 133.4, 113.7 ppm.

##### Synthesis of 4,7-diphenyl-2,1,3-benzothiadiazole (**2a**) and 4-bromo-7-phenyl-2,1,3-benzothiadiazole (**2b**)

To a 250 mL two-necked round-bottomed flask were added compound **1** (1 g, 3.40 mmol) in 32 mL of benzene and Na<sub>2</sub>CO<sub>3</sub> (2 M, 21 mL). A solution of phenylboronic acid (415 mg, 3.73 mmol) in 15 mL of ethanol was added to two-necked flask at 60 °C under an argon atmosphere. Pd(PPh<sub>3</sub>)<sub>4</sub> catalyst (118 mg, 0.10 mmol) was added to the solution and the solution was stirred at 80 °C for 15 h. Small amount of water was poured into the solution. The reaction mixture was extracted with chloroform and concentrated under vacuum. The resulting green solid was purified by column chromatography on silica gel using dichloromethane:*n*-hexane (3:2) as an eluent. However, the mixture of **2a** and **b** were not separated from each other. They were used as a mixture in the

next step. Only a small amount of compound **2a** was isolated for the analysis. Yield for **2a** and **b** mixture: 80%, FT-IR (KBr pellet,  $\text{cm}^{-1}$ ): 3448, 3056, 3033, 2957, 2925, 1527, 1478, 1447, 1328, 1266, 1184, 1154, 1075, 1031, 933, 882, 843, 790, 757, 694, 517  $\text{cm}^{-1}$ .  $^1\text{H}$  NMR (400 MHz,  $\text{CDCl}_3$   $\delta$  7.22 ppm):  $\delta$  = 7.96 (4H, d,  $J$  = 7.6 Hz), 7.76 (2H, s), 7.53 (4H, t,  $J$  = 7.6 Hz), 7.44 (2H, t,  $J$  = 7.6 Hz) ppm.  $^{13}\text{C}$  NMR [100 MHz,  $\text{CDCl}_3$   $\delta$  78.8 (3 peaks)]:  $\delta$  = 154.3, 137.6, 133.6, 129.4, 128.8, 128.5, 128.3 ppm.

#### Synthesis of [1,1':4,1'']-terphenyl-2',3'-diamine (**3a**) and 4-bromobiphenyl-2,3-diamine (**3b**)

To the mixture of **2a–b** (1 g) in 120 mL of ethanol:THF (3:1) solution was added  $\text{CoCl}_2 \cdot 6\text{H}_2\text{O}$  (11.3 mg, 47.5  $\mu\text{mol}$ ) and  $\text{NaBH}_4$  (144 mg, 3.81 mmol), respectively. The mixture was stirred at 80 °C under an argon atmosphere for 20 h. Black solid  $\text{Co}_2\text{B}$  was formed instantly and, in a few minutes,  $\text{H}_2\text{S}$  evolution was noted. Then, the solution was cooled to room temperature and filtered off. The black solid was separated and then solvent was evaporated. 50 mL of water was poured into the solution and the reaction mixture was extracted with  $\text{Et}_2\text{O}$ . The solid product couldn't be purified by column chromatography because the diamine product does not stable in air. Diamines were used immediately in the next step to avoid fast decomposition.

#### Synthesis of 2-(4-bromo-7-phenyl-1H-benzimidazole-2-yl)phenol (**BI**)

To the mixture of **3a–b** (1.3 g) and salicylaldehyde (579  $\mu\text{L}$ , 5.43 mmol) were dissolved in 25 mL of acetonitrile.  $\text{CoCl}_2 \cdot 6\text{H}_2\text{O}$  (120 mg, 0.50 mmol) was added to the reaction mixture and the mixture was stirred at room temperature overnight. After completion, the solvent was evaporated and the crude product was dissolved in 25 mL of ethanol and then treated with 2 mL of  $\text{NH}_4\text{OH}$ , followed by 25 mL of water. The mixture was heated and then cooled to room temperature and then the precipitate was washed with solvent mixture of *n*-hexane/ethanol. The crude solid was purified by column chromatography on silica gel using dichloromethane:*n*-hexane (3:2) as an eluent. Yield: 95%, FT-IR (KBr pellet,  $\text{cm}^{-1}$ ): 3420, 3062, 2918, 1628, 1595, 1488, 1417, 1384, 1257, 1219, 772, 698  $\text{cm}^{-1}$ .  $^1\text{H}$  NMR (400 MHz,  $\text{DMSO}-d_6$   $\delta$  2.47 ppm):  $\delta$  = 13.28 (1H, s), 8.07 (1H, d,  $J$  = 3.4 Hz), 7.96 (1H, d,  $J$  = 7.1 Hz), 7.59 (1H, d,  $J$  = 7.7 Hz), 7.51 (2H, t,  $J$  = 7.1 Hz), 7.38 (4H, m), 7.02 (2H, d,  $J$  = 7.7 Hz) ppm.  $^{13}\text{C}$  NMR [100 MHz,  $\text{DMSO}-d_6$   $\delta$  40.2 ppm (7 peaks)]:  $\delta$  = 168.7, 162.6, 138.6, 132.4, 129.2, 129.1, 128.1, 126.8, 124.4, 122.0, 119.7, 117.8, 113.1, 111.4 ppm.

#### Synthesis of 2-(2-Hydroxyphenyl)-7-phenyl-1H-benzimidazole-4-boronic acid (**BI-B(OH)<sub>2</sub>**)

Compound **BI** (110 mg, 0.30 mmol) was dissolved in 7 mL of THF and the solution was cooled to  $-78$  °C in cooling bath of dry ice/acetone. *n*-butyllithium solution (1.6 M in *n*-hexane, 1 mL, 1.6 mmol) was added dropwise to solution under an argon atmosphere. The mixture was stirred at  $-78$  °C for 1 h and then trimethyl borate (89  $\mu\text{L}$ , 0.80 mmol) was added to solution slowly. The solution was cooled to room temperature within the time period of 3 h and then stirred at room temperature overnight. The solution was cooled to 0 °C and pH of the solution was adjusted to 2–3 by adding 2 M of HCl solution. The reaction mixture was extracted with THF. Yield: 75%, FT-IR (KBr pellet,  $\text{cm}^{-1}$ ): 3218 (boronic acid O–H stretching), 2958, 2927, 2866, 1630, 1557, 1385 ( $\nu_{\text{B-O}}$ ), 1265, 1152, 1060, 772, 757, 700  $\text{cm}^{-1}$ .

#### Synthesis of *N,N'*-bis(2,6-diisopropylphenyl)-1,7-bis[2-(2-hydroxyphenyl)-7-phenyl-1H-benzimidazole-4-yl]perylene-3,4,9,10-tetracarboxylic diimide (**BI-PDI**)

To a 50 mL two-necked round-bottomed flask were added **P2** dye (50 mg, 0.058 mmol) in 6 mL of benzene and  $\text{Na}_2\text{CO}_3$  (2 M, 3 mL). A solution of compound **BI-B(OH)<sub>2</sub>** (40 mg, 0.12 mmol) in

3 mL of ethanol was added to two-necked flask at 80 °C under an argon atmosphere.  $\text{Pd}(\text{PPh}_3)_4$  catalyst (3 mg, 2.6  $\mu\text{mol}$ ) was added to the mixture and then the solution was stirred at 80 °C for 72 h. Finally, the solvent was evaporated. The crude product was purified by column chromatography on silica gel using dichloromethane:*n*-hexane (10:1) as an eluent. Yield: 80%, FT-IR (KBr pellet,  $\text{cm}^{-1}$ ): 3402 (O–H stretching), 2962 and 2926 (aliphatic  $\nu_{\text{C-H}}$ ), 1704 (imide  $\nu_{\text{C=O}}$ ), 1666 (imide  $\nu_{\text{C=O}}$ ), 1592 (aromatic  $\nu_{\text{C=C}}$ ), 1464, 1422, 1344 ( $\nu_{\text{C-N}}$ ), 1264, 1202, 942, 810, 750  $\text{cm}^{-1}$ .  $^1\text{H}$  NMR (400 MHz,  $\text{CDCl}_3$   $\delta$  7.26 ppm):  $\delta$  = 9.78 (2H, d,  $J$  = 8.4 Hz), 8.81 (3H, d,  $J$  = 2.2 Hz), 8.79 (4H, d,  $J$  = 2.2 Hz), 8.77 (2H, s), 8.74 (2H, s), 8.72 (1H, s), 8.69 (2H, d,  $J$  = 8.4 Hz), 8.59 (2H, s), 7.60 (6H, m), 7.36 (10H, m), 2.77 (4H, septet,  $J$  = 6.8 Hz), 1.19 (24H, d,  $J$  = 6.8 Hz) ppm.  $^{13}\text{C}$  NMR [100 MHz,  $\text{CDCl}_3$   $\delta$  77.2 (3 peaks)]:  $\delta$  = 164.0, 163.8, 163.6, 158.2, 146.9, 146.8, 136.4, 136.3, 136.1, 134.7, 132.6, 131.6, 131.2, 131.1, 130.9, 130.7, 130.0, 129.9, 129.8, 129.7, 129.1, 128.9, 127.7, 124.3, 124.2, 124.0, 123.2, 122.4, 119.6, 29.4, 24.2 ppm.

## Results and discussion

### Optical properties

**BI-PDI** dye exhibits three characteristic PDI core absorption bands between 480 and 560 nm belonging to its electronic  $S_0$ – $S_1$  transition in solutions. Also, absorption bands in the region of 380–410 nm are attributed to its electronic  $S_0$ – $S_2$  absorption indicating the  $\pi$ – $\pi^*$  transition of the aromatic rings. The maximum and the shoulder of the absorption band of **BI-PDI** in more polar ethanol and benzonitrile solutions are shifted to blue and red region, respectively, as shown in Fig. 1a. No aggregation behavior was observed in studied solutions according to the absorption spectra. Fig. 1b illustrates the steady-state emission spectra of **BI-PDI** in different solvents of increasing polarities. Higher the polarities of the solvents, the more increase the red shifted wavelength of emission maxima of the dye. In ethanol solution, charge transfer is enhanced by the intra- or inter-molecular hydrogen bond formation with the unshared electron pairs of the heteroatoms on benzimidazole group of the dye. This leads to significant shift to longer wavelength on its emission spectrum. Larger Stokes shift (Table 1) in ethanol solution with respect to other solutions supports the change in electronic spectra, leading to the possible formation of excimer for perylene core. Fig. 1c illustrates the decays of single photon timing experiments in Bz-Cl solution. Decay analysis in both less polar Bz-Cl and more polar Bz-CN solutions gave two-exponential decays at the emission wavelength of 570 nm for **BI-PDI** as summarized in Table 2. Fast decay components at 0.47 and 0.86 may be attributed to the photoinduced energy hopping process between the different **BI-PDI** conformers generated because of deformation of its molecular planarity. The occurrence of faster energy trapping may be explained by the through-space orientation of benzimidazole subunits toward to the perylene core. Other decay values at 4.54 and 4.70 in solutions may be attributed to the stationary fluorescence of PDI. Energy transfer from the perylene core to the benzimidazole group is unlikely at the excitation wavelength of 485 nm, because  $S_1$  state of PDI chromophore is lower than that of benzimidazole subunit.

Thin films of **BI-PDI**, BI-PDI:PC<sub>61</sub>BM and P3HT:BI-PDI blends (as shown in Fig. 1a, Fig. 2a and b, respectively) are prepared by doctor blading 2 wt% Bz-Cl solution to form films. The absorption spectrum of **BI-PDI** gives a maximum signal at 571 nm and a shoulder at 530 nm originating from the PDI core absorption. The absorption spectrum of 1:1 (w:w) ratio of blend film for BI-PDI:PC<sub>61</sub>BM displays maxima at 564 nm with a shoulder at 525 nm and gives a marked hypsochromic shift (about 5–7 nm) in maxima compared

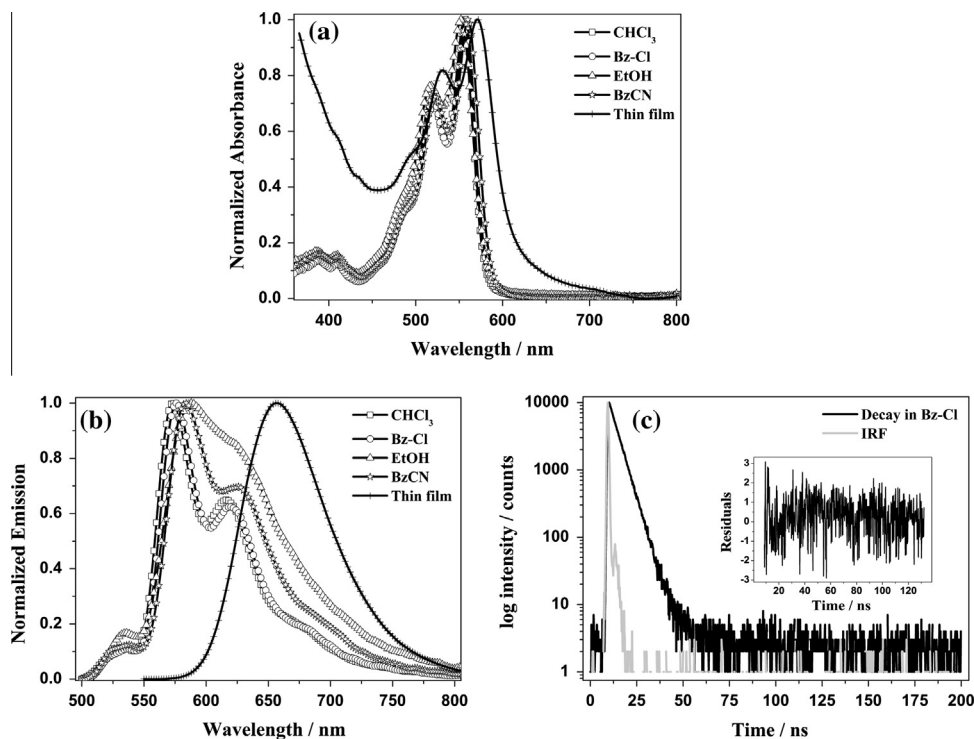


**Fig. 1.** Normalized (a) UV–Vis absorption and, (b) fluorescence spectra of **BI-PDI** dye in solvents of different polarities at the concentrations of  $10^{-6}$  mol/L and on thin films ( $\lambda_{\text{exc}} = 485$  nm). (c) Fluorescence decay of **BI-PDI** dye in chlorobenzene ( $\lambda_{\text{detection}} = 570$  nm, time increment = 194 ps).

**Table 1**

The UV–visible absorptions, fluorescence emissions and Stokes shifts ( $\text{cm}^{-1}$ ) data of **BI-PDI** in solvents of different polarities and on thin films ( $\lambda$  (nm),  $\epsilon$  ( $\text{L mol}^{-1} \text{cm}^{-1}$ )) ( $\lambda_{\text{exc}} = 485$  nm).

Solvent	$\epsilon^a$	$\lambda_1$	$\lambda_2$	$\lambda_3$	$\lambda_{4(\text{max})}$	$\lambda_{\text{em}(\text{max})}$	$(\nu_A - \nu_F)$
Chloroform	4.8	387	409	517	555	573	566
Chlorobenzene	5.6	388	409	519	557	576	592
Ethanol	24.5	386	410	517	552	588	1109
Benzonitrile	26.0	389	411	522	560	583	704
Thin films	–	–	–	530	571	656	2269

<sup>a</sup> Dielectric constant values were taken from the Ref. [47].

**Table 2**

Fluorescence decay times ( $\tau_{f(i)}$  (ns)) and associated relative amplitudes ( $\alpha_i$  (%))<sup>a</sup> and fluorescence lifetimes ( $\tau_f$  (ns)) of **BI-PDI** in chlorobenzene and benzonitrile solutions ( $\lambda_{\text{exc}} = 485$  nm).

<b>BI-PDI</b>	$\tau_{f(1)}$	$\alpha_1$	$\tau_{f(2)}$	$\alpha_2$	$\tau_f$
Chlorobenzene	0.47	4.1	4.54	95.9	2.51
Benzonitrile	0.86	5.0	4.70	95.0	2.78

<sup>a</sup> Relative amplitude values,  $\alpha_i$ , were calculated with the formula [48]:  $W\alpha_i = \tau_f \times P_i / \sum \tau_i \times P_i$ , where  $\tau_i$  was the decay time of the compound, and  $P_i$  was the number of free parameters in the fit function ( $\lambda_{\text{detection}} = 575$  nm,  $\chi^2 = 1.1$ ). Fluorescence life times are calculated with the formula:  $\tau_f = \sum \tau_{f(i)} / n$ .

to the same spectrum for pristine **BI-PDI**. Absorption spectra for thermally annealed films of P3HT:BI-PDI blends give the same absorption maxima like pristine **BI-PDI** dye. However, it can be seen from the Fig. 2b that both the intensity and the shape of the signal are changed. These differences may be explained by the aggregation behavior of PDI dye and the occurrence of the donor–acceptor electronic interactions.

The emission of **BI-PDI** on thin film is centered at 656 nm, as shown in Fig. 2c. The other observed peaks can be attributed to the emission of PDI and P3HT films which were thermally annealed

blends. The addition of P3HT to the **BI-PDI** results in the generation of new emission peaks at 724 nm and bathochromic shifts at the absorption maximum of **BI-PDI** from 656 to 666 nm. Both the shifting of PDI emission maximum and also broad shape of the emission peak support the aggregation behavior of **BI-PDI** dye. Photoluminescence studies indicate that  $\pi$ – $\pi$  stacking of P3HT is disturbed by blending with **BI-PDI** dye.

#### CV measurements

Fig. 3 illustrates the cyclic voltammograms of **BI** and **BI-PDI** dyes and the results are given in Table 3. **BI-PDI** dye gives reduction waves at  $-0.43$  and  $-0.65$  V, indicating the formation of stable PDI monoanion and dianion radicals, respectively. Those values are well-correlated with reference values for bay-substituted PDI dyes in the literature [35]. Also, **BI** dye exhibits oxidation wave at 1.25 V and reduction wave at  $-1.21$  V, indicating the formation of benzimidazole cation and anion radical, respectively. There is a good correlation between the experimentally ( $\sim 2.01$  eV) and theoretically calculated ( $\sim 2.10$  eV) band gap values indicating the  $S_0$ – $S_1$  transition of **BI-PDI** dye in solution. The HOMO energy level of **BI-PDI** dye is calculated to be about  $-5.92$  eV. HOMO level of the dye is lower than that of the HOMO level of the P3HT ( $\sim -5.1$  eV) molecule, indicating the more efficient hole transfer from PDI to P3HT structure. The corresponding LUMO energy level of **BI-PDI** dye is estimated to be  $-3.82$  eV which is slightly higher than that of PC<sub>61</sub>BM ( $\sim -3.9$  eV) molecule. Also, **BI-PDI** dye has a suitable energy level as p-type organic semiconductor material towards to PC<sub>61</sub>BM small molecule for OPV devices.

#### Atomic force microscopy (AFM) images

To gain a better understanding of surface morphology which gives us important data to form optimized structure of the device, we have used atomic force microscopy images. Fig. 4a and b show

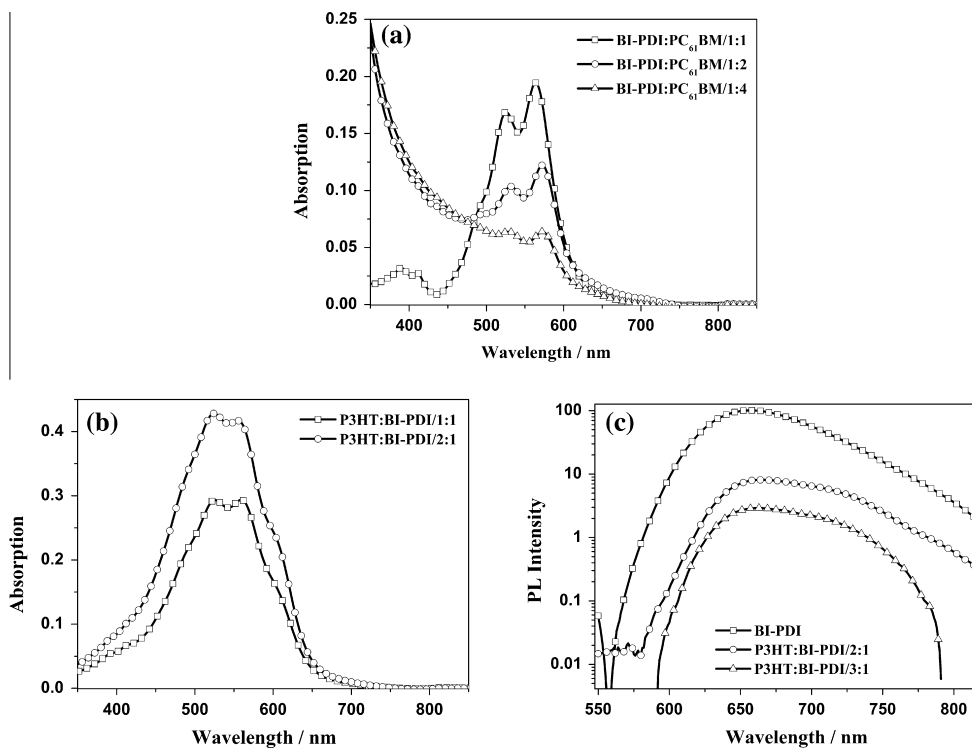


**Fig. 2.** Ground state absorption spectra obtained on thin films of (a) BI-PDI:PC<sub>61</sub>BM and, (b) P3HT:BI-PDI blends under investigation. (c) Normalized steady-state photoluminescence spectra of pristine BI-PDI dye and P3HT:BI-PDI blend films ( $\lambda_{\text{exc}} = 485$  nm).

**Table 3**

Cyclic voltammeter data and molecular orbital energies of BI and BI-PDI dye with respect to the vacuum level.<sup>a</sup>

Dye	$E_{\text{red}2}^0$ (V)	$E_{\text{red}1}^0$ (V)	$E_{\text{ox}1}^0$ (V)	LUMO-1 (eV)	LUMO (eV)	HOMO <sup>b</sup> (eV)	$E_{\text{gap}}$ (eV)
BI		-1.21	1.25	-	-3.04	-5.69	2.65
BI-PDI	-0.65	-0.43	1.58	-3.6	-3.82	-5.92	2.10

<sup>a</sup> HOMO and LUMO energy levels of the dyes were determined by the formulas:  $E_{\text{LUMO}} = -(4.8 + E_{\text{red}}^{\text{onset}})$ ,  $E_{\text{red}}^{\text{onset}} = E_{\text{red}}^0 - E_{\text{ox}}^0(\text{ferrocene})$ ,  $E_{\text{HOMO}} = E_{\text{LUMO}} - E_{\text{gap}}$  [49].

<sup>b</sup> Band gap values were calculated from the onset values of the absorption bands.

the AFM images of thermally annealed BI-PDI:PC<sub>61</sub>BM (1:4, w/w) and P3HT:BI-PDI (3:1, w/w) films, and also Fig. 4c shows BI:PC<sub>61</sub>BM (1:2, w/w) blend films which are taken after device fabrication. As seen, the root-mean-square (rms) roughness of BI-PDI:PC<sub>61</sub>BM blend is smaller than that of P3HT:BI-PDI blend film. The rms roughness of the active layers were 0.40 nm for BI-PDI:PC<sub>61</sub>BM, 2.01 nm for P3HT:BI-PDI and 0.47 nm for BI:PC<sub>61</sub>BM, respectively. It is concluded that the addition of BI-PDI dye to P3HT polymer reduces the  $\pi$ - $\pi$  interaction of PDI structure with polymeric backbone.

It is known that highly twisted geometric structure of bay-substituted PDI molecules may adversely impact on molecular packing and thin film morphology [38]. Also, similar rotation was observed for benzimidazole substituted BI-PDI dye, which may inhibits the regular  $\pi$ - $\pi$  stacking of perylene core with thiophene rings of P3HT structure when blending with the polymer.

#### Device performance and external quantum efficiency (EQE)

PDI's not only can be used as n-type semiconductor towards donor materials, but also they can be employed as p-type semiconductor in OPV devices. There is no sufficient data about the PDI's performance as p-type material in OPV devices in literature. Only a few reports are seen concerning OPV structures using perylenes as donor material towards acceptors. Choi and co-workers have

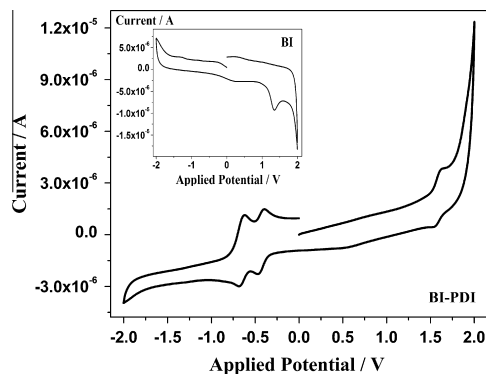


**Fig. 3.** Cyclic voltammograms of BI-PDI dye in 0.1 M [TBA][PF<sub>6</sub>]/Me-CN at 50 mV/s scan rate on glassy carbon working electrode. Inset shows BI voltammogram.

obtained maximum PCE of 1.60% by using PDI type donor-acceptor structure containing  $\pi$ -extended structure that are incorporated into the perylene units [50].

Benzimidazole substitution in 1-,7-positions for BI-PDI small molecule is a good choice to minimize the aggregation effect of PDI molecule. Also, the charge recombination between PDI molecules may be minimized by substitution of functional groups in

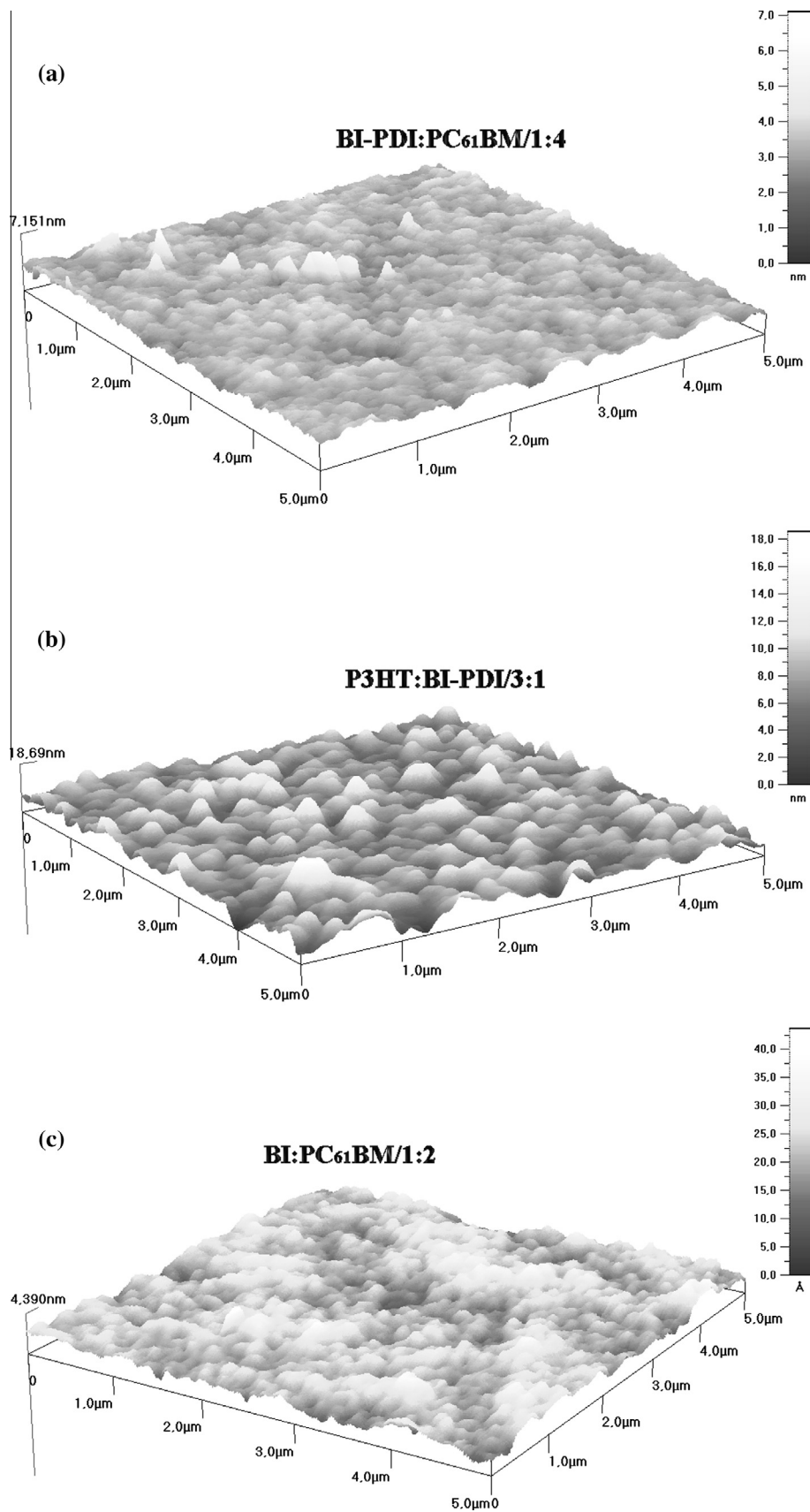


**Fig. 4.** Representative AFM images of (a) BI-PDI:PC<sub>61</sub>BM (1:4, w/w), (b) P3HT:BI-PDI (3:1, w/w) and (c) BI:PC<sub>61</sub>BM (1:2, w/w) blend films on the glass substrate coated from chlorobenzene.

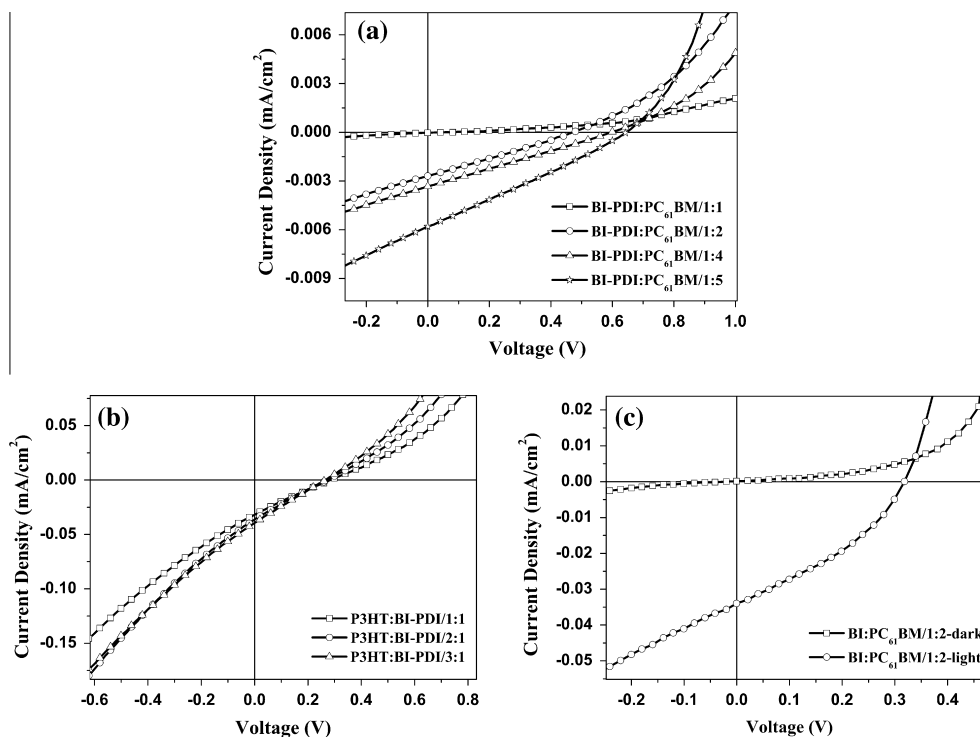


Fig. 5.  $I$ - $V$  curves of photovoltaic devices using (a) BI-PDI:PC<sub>61</sub>BM, (b) P3HT:BI-PDI and (c) BI:PC<sub>61</sub>BM blends as active layers.

Table 4

Photovoltaic parameters of ITO/PEDOT:PSS/Active Layer/Ca(15 nm)/Ag(80 nm) bulk heterojunction solar cells.

Active Layer		$V_{oc}$ (V)	$I_{sc}$ (mA/cm <sup>2</sup> )	FF (%)	$\eta$ ( $\times 10^{-3}$ %)
Donor:acceptor	w:w				
P3HT:PC <sub>61</sub> BM	1:1	0.55	7.91	61.3	2720
BI-PDI:PC <sub>61</sub> BM	1:1	0.08	0.0003	9.4	0.002
	1:2	0.47	0.025	26.0	3.2
	1:4	0.60	0.032	25.4	4.8
	1:5	0.64	0.055	27.2	9.7
	P3HT:BI-PDI	1:1	0.28	0.032	23.8
P3HT:BI-PDI	2:1	0.28	0.036	22.8	2.3
	3:1	0.26	0.039	24.9	2.5
BI:PC <sub>61</sub> BM	1:2	0.31	0.033	35.8	3.9

Table 5

SCLC hole and electron mobilities of different combinations of thin film cast from chlorobenzene solvent.

Solar cell structure		Hole mobility ( $\mu$ , cm <sup>2</sup> /Vs)	Electron mobility ( $\mu$ , cm <sup>2</sup> /Vs)
Donor:acceptor	w:w		
BI-PDI:PC <sub>61</sub> BM	1:5	$3.70 \times 10^{-6}$ ( $R^2:0.99$ )	
BI:PC <sub>61</sub> BM	1:2	$1.01 \times 10^{-6}$ ( $R^2:0.99$ )	
P3HT:BI-PDI	3:1		$2.58 \times 10^{-5}$ ( $R^2:0.99$ )

bay positions of the perylene core [38]. Do and co-workers have modified a perylene dye to imide-imidazole derivative comprised of a benzimidazole moiety giving a PCE of 0.20% with the increase in perylene content [51].

In the first type of device production, BI-PDI small molecule is used as donor material in typical sandwich configuration of ITO/PEDOT:PSS/BI-PDI:PC<sub>61</sub>BM/Ca/Ag (Fig. 5a) instead of P3HT polymer. Because absorption band of P3HT almost overlaps with the shape of the absorption spectrum of BI-PDI dye in the visible region so that BI-PDI dye may collect the visible photon-flux at least similar to P3HT polymer. The open-circuit voltage ( $V_{oc}$ ), short-circuit current ( $I_{sc}$ ), fill factor (FF) and power conversion efficiency ( $\eta$ )

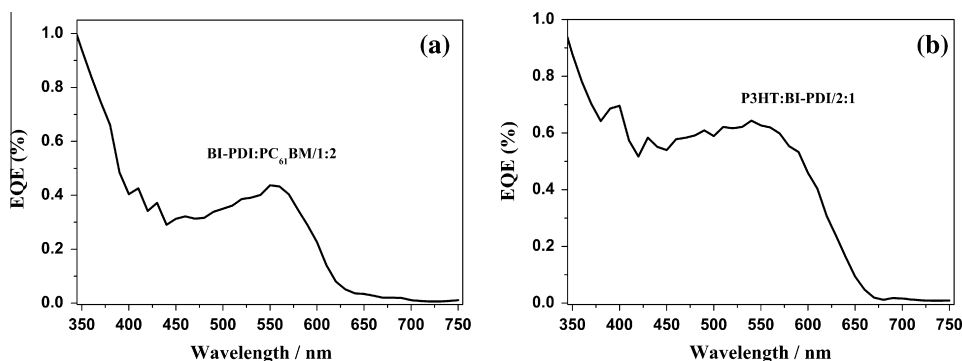
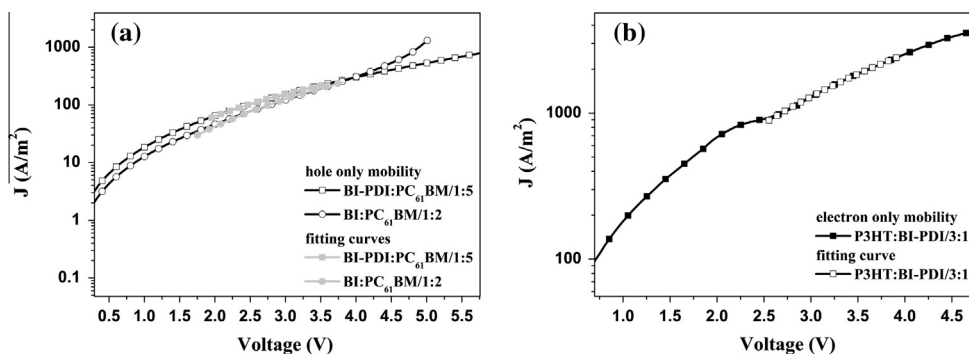


Fig. 6. EQE spectra of (a) BI-PDI:PC<sub>61</sub>BM (1:2, w/w) and (b) P3HT:BI-PDI (2:1, w/w) under investigation.



**Fig. 7.** Dark current density-effective voltage characteristics of SCLC mobilities in (a) BI-PDI:PC<sub>61</sub>BM (1:5, w/w) and BI:PC<sub>61</sub>BM (1:2, w/w) and, (b) P3HT:BI-PDI (3:1, w/w) thin film cast from chlorobenzene.

of all the device combinations are summarized in Table 4. The best device using **BI-PDI** small molecule as donor with donor:acceptor weight ratio of 1:5 exhibits a  $V_{OC}$  of 0.64 V,  $I_{SC}$  of 0.055 mA/cm<sup>2</sup> and FF value of 27.2 with PCE of 0.01.  $I_{SC}$  and  $V_{OC}$  values of the devices improve when PC<sub>61</sub>BM content of active layer blend increases. These low efficiencies may be related to the weak interaction of fullerene additive with the perylene core which is rotated out of plane with bulky benzimidazole substituent due to steric hindrance. However, PDI structure shows better  $\pi$ - $\pi$  interaction when the PC<sub>61</sub>BM content is increased in the blend. Finally, charge injection increase and efficiencies can reach to slightly higher values. Fig. 5b illustrates the  $I$ - $V$  curves of the second type of device with ITO/PEDOT:PSS/P3HT:BI-PDI/Ca/Ag configuration, where **BI-PDI** was used as acceptor. PCE values of the devices are very low and are not affected by the differences in blend ratios of the active layer. PDI molecules aggregate in the presence of P3HT polymer, as understood from PL experiments. This generates intermolecular recombination centers which inhibit the charge injection.

We have also tried device performance of pristine **BI** structure in the device configuration of ITO/PEDOT:PSS/BI:PC<sub>61</sub>BM/Ca/Ag in order to understand the benzimidazole group effect on photovoltaic performance (Fig. 5c). In our study, **BI** structure in device gives a FF of 35.8, which is lower than that of **BI-PDI** small molecule.

The external quantum efficiency (EQE) curves of BI-PDI:PC<sub>61</sub>BM and P3HT:BI-PDI devices under illumination are shown in Fig. 6a and 6b, respectively. The EQEs of the device cover the most of the visible region wavelength in the range from 400 to 700 nm for both configurations. Contribution of visible light to photocurrent is only about 0.44% in blend of **BI-PDI** with PC<sub>61</sub>BM device. In the presence of P3HT films blended with the **BI-PDI** dye, the EQE value is enhanced in the PDI region and reaches to its highest value of 0.64%, which results from the overlap of PDI signal with P3HT absorption in the same visible region. Although the EQE shows relatively better overlap of the absorption spectrum with the solar spectrum, its value is extremely low in order to absorb sufficient light.

#### Transport studies

The hole and electron mobilities of the components for the active layers play an important role in discussing the photovoltaic performance of the device [52,53]. We have used the space charge limited current (SCLC) [54] regime to get information about the **BI-PDI** small molecule and other blends given in Table 5. We have fabricated the devices in a configuration of ITO/AZO(HT)/Active Layer/Ca/Ag for electron mobilities and ITO/PEDOT:PSS/Active Layer/PEDOT:PSS/Ag for hole mobilities. Fig. 7a shows  $I$ - $V$  characteristics of SCLC

mobilities in BI-PDI:PC<sub>61</sub>BM and BI:PC<sub>61</sub>BM. The hole mobilities for BI-PDI:PC<sub>61</sub>BM and BI:PC<sub>61</sub>BM blends are found to be  $3.70 \times 10^{-6}$  and  $1.01 \times 10^{-6}$  cm<sup>2</sup>/Vs, respectively. Also, electron mobility for P3HT:BI-PDI blend is found to be about  $2.58 \times 10^{-5}$  cm<sup>2</sup>/Vs (Fig. 7b).

In generally, electron and hole mobilities of the devices are very low and in the order of  $10^{-6}$  cm<sup>2</sup>/Vs, which explain the poor efficiencies of the BHJ solar cells. The low mobilities may be related to the non-planar structure of PDI core which reduces the inter-chain  $\pi$ - $\pi$  interactions [55]. These interactions may be inhibited by the bulky benzimidazole group in bay positions of the perylene ring. It seems to be electron mobilities of **BI-PDI** small molecule in blends are approximately ten times higher than hole mobilities of **BI-PDI** dye so that this dye is more suitable to be used as acceptor material in given components.

#### Conclusions

In this study, we have tried to disrupt the planarity of the perylene core and also to prevent the aggregate formation by attaching bulk benzimidazole groups in bay positions of the central ring for the purpose of application in solution-processed BHJ solar cell. All OPVs based on **BI-PDI** small molecule as donor and PC<sub>61</sub>BM as acceptor or P3HT as donor and **BI-PDI** as acceptor have been investigated systematically. PL and absorption measurements support the aggregation tendency of **BI-PDI** dye in the presence of P3HT polymer, which results the deformation of  $\pi$ - $\pi$  stacking of P3HT polymer with perylene core giving poor efficiencies. In the device of BI-PDI:PC<sub>61</sub>BM blend, **BI-PDI** dye exhibits weak interaction with fullerene due to the rotation out of plane resulting poor efficiencies. EQE and electron/hole mobility measurements also indicate these low performances.

Twisted form of **BI-PDI** dye caused by bulk benzimidazole group does not help to increase the short circuit current density and device efficiency. Potential reason for those observations may be related to the weak interaction of the dye with the components when it is blended. In summary, twisted form, molecular shape and morphology of **BI-PDI** dye play a promising role in BHJ solar cell performance. Hence the morphological properties of donor-acceptor couple will remain a highly essential issue for the next researches.

#### Acknowledgements

Financial support for this work was provided by the Research Council of Celal Bayar University (BAP/2011-056) and the High Education Council of Turkey. We thank to the State Planning Organization of Turkey (DPT).

## References

- [1] Y. Lin, Y. Li, X. Zhan, *Chem. Soc. Rev.* 41 (2012) 4245–4272.
- [2] X.H. Zhu, J. Peng, Y. Cao, J. Roncali, *Chem. Soc. Rev.* 40 (2011) 3509–3524.
- [3] H.-S. Shim, H.J. Kim, J.W. Kim, S.-Y. Kim, W.-I. Jeong, T.-M. Kim, J.-J. Kim, *J. Mater. Chem.* 22 (2012) 9077–9081.
- [4] B.P. Rand, D. Cheyng, K. Vasseur, N.C. Giebink, S. Mothy, Y. Yi, V. Coropceanu, D. Beljonne, J. Cornil, J.-L. Brédas, J. Genoe, *Adv. Funct. Mater.* 22 (2012) 2987–2995.
- [5] S.Y. Leblebici, L. Catane, D.E. Barclay, T. Olson, T.L. Chen, B. Ma, *ACS Appl. Mater. Interfaces* 3 (2011) 4469–4474.
- [6] T. Mueller, R. Gresser, K. Leo, M. Riede, *Sol. Energy Mater. Sol. Cells* 99 (2012) 176–181.
- [7] V.S. Barlier, C.W. Schlenker, S.W. Chin, M.E. Thompson, *Chem. Commun.* 47 (2011) 3754–3756.
- [8] L. Valentini, D. Bagnis, A. Marrocchi, M. Seri, A. Taticchi, J.M. Kenny, *Chem. Mater.* 20 (2008) 32–34.
- [9] K.N. Winzenberg, P. Kemppinen, G. Fanchini, M. Bown, G.E. Collis, C.M. Forsyth, K. Hegedus, T.B. Singh, S.E. Watkins, *Chem. Mater.* 21 (2009) 5701–5703.
- [10] Q.Q. Shi, P. Cheng, Y.F. Li, X.W. Zhan, *Adv. Energy Mater.* 2 (2012) 63–67.
- [11] P. Dutta, W. Yang, W.H. Lee, I.N. Kang, S.H. Lee, *J. Mater. Chem.* 22 (2012) 10840–10851.
- [12] P. Dutta, W. Yang, S.H. Eom, S.H. Lee, *Org. Electron.* 13 (2012) 273–282.
- [13] J. Zhang, J. Yu, C. He, D. Deng, Z.-G. Zhang, M. Zhang, Z. Li, Y. Li, *Org. Electron.* 13 (2012) 166–172.
- [14] S. Qu, H. Tian, *Chem. Commun.* 48 (2012) 3039–3051.
- [15] G.D. Sharma, J.A. Mikroyannidis, S.S. Sharma, M.S. Roy, K.R. Justin, Thomas, *Org. Electron.* 13 (2012) 652–666.
- [16] J.G. Mei, K.R. Graham, R. Stalder, J.R. Reynolds, *Org. Lett.* 12 (2010) 660–663.
- [17] A. Iwan, E. Schab-Balcerzak, M. Siwy, A. Sikora, M. Palewicz, H. Janeczek, M. Sibinski, *Opt. Mater.* 33 (2011) 958–967.
- [18] J. Roncali, *Chem. Soc. Rev.* 34 (2005) 483–495.
- [19] X. Zhan, A. Facchetti, S. Barlow, T.J. Marks, M.A. Ratner, M.R. Wasielewski, S.R. Marder, *Adv. Mater.* 23 (2011) 268–284.
- [20] P.E. Keivanidis, I.A. Howard, R.H. Friend, *Adv. Funct. Mater.* 18 (2008) 3189–3202.
- [21] E. Kozma, M. Catellani, *Dyes Pigm.* 98 (2013) 160–179.
- [22] C. Zafer, M. Kus, G. Turkmen, H. Dincalp, S. Demic, B. Kuban, Y. Teoman, S. Icli, *Sol. Energy Mater. Sol. Cells* 91 (2007) 427–431.
- [23] H. Quante, Y. Geerts, K. Mullen, *Chem. Mater.* 9 (1997) 495–500.
- [24] H. Langhals, J. Karolin, L.B.A. Johansson, *J. Chem. Soc. Faraday Trans.* 94 (1998) 2919–2922.
- [25] H. Dinçalp, S. İcli, *Sol. Energy* 80 (2006) 332–346.
- [26] D.K. Susarova, P.A. Troshin, D. Höglinger, R. Koeppel, S.D. Babenko, R.N. Lyubovskaya, V.F. Razumov, N. Serdar Sariciftci, *Sol. Energy Mater. Sol. Cells* 94 (2010) 803–811.
- [27] G.D. Sharma, P. Balraju, J.A. Mikroyannidis, M.M. Stylianakis, *Sol. Energy Mater. Sol. Cells* 93 (2009) 2025–2028.
- [28] W.S. Shin, H.-H. Jeong, M.-K. Kim, S.-H. Jin, M.-R. Kim, J.-K. Lee, J.W. Lee, Y.-S. Gal, *J. Mater. Chem.* 16 (2006) 384–390.
- [29] V. Kamm, G. Battagliarin, I.A. Howard, W. Pisula, A. Mavrinskiy, C. Li, K. Müllen, F. Laquai, *Adv. Energy Mater.* 1 (2011) 297–302.
- [30] W. Fu, C. He, Z. Li, *J. Polym. Sci. A1* (50) (2012) 1333–1341.
- [31] P.E. Keivanidis, V. Kamm, W. Zhang, G. Floudas, F. Laquai, I. McCulloch, D.D.C. Bradley, J. Nelson, *Adv. Funct. Mater.* 22 (2012) 2318–2326.
- [32] X. Guo, L. Bu, Y. Zhao, Z. Xie, Y. Geng, L. Wang, *Thin Solid Films* 517 (2009) 4654–4657.
- [33] G.D. Sharma, P. Suresh, J.A. Mikroyannidis, M.M. Stylianakis, *J. Mater. Chem.* 20 (2010) 561–567.
- [34] S. Jeong, Y.S. Han, Y. Kwon, M.-S. Choi, G. Cho, K.-S. Kim, Y. Kim, *Synth. Met.* 160 (2010) 2109–2115.
- [35] C.C. Chao, M.K. Leung, Y.O. Su, K.Y. Chiu, T.H. Lin, S.J. Shieh, S.C. Lin, *J. Org. Chem.* 70 (2005) 4323–4331.
- [36] M. Queste, C. Cadiou, B. Pagoaga, L. Giraudet, N. Hoffmann, *New J. Chem.* 34 (2010) 2537–2545.
- [37] G. Türkmen, S. Erten-Ela, S. Icli, *Dyes Pigm.* 83 (2009) 297–303.
- [38] C. Li, H. Wonnerberger, *Adv. Mater.* 24 (2012) 613–636.
- [39] S. Song, H. Han, Y. Kim, B.H. Lee, S.H. Park, Y. Jin, I. Kim, K. Lee, H. Suh, *Sol. Energy Mater. Sol. Cells* 95 (2011) 1838–1845.
- [40] F.S. Mancilha, B.A. DaSilveira Neto, A.S. Lopes, P.F. Moreira, F.H. Quina, R.S. Gonçalves, J. Dupont, *Eur. J. Org. Chem.* 2006 (2006) 4924–4933.
- [41] A.S.D. Sandanayaka, K. Matsukawa, T. Ishi-i, S. Mataka, Y. Araki, O. Ito, *J. Phys. Chem. B* 108 (2004) 19995–20004.
- [42] B.A.D. Neto, A.S. Lopes, M. Wust, V.E.U. Costa, G. Ebeling, J. Dupont, *Tetrahedron Lett.* 46 (2005) 6843–6846.
- [43] A.T. Khan, T. Parvin, L.H. Choudhury, *Synth. Commun.* 39 (2009) 2339–2346.
- [44] S.-J. Liu, Q. Zhao, Q.-L. Fan, W. Huang, *Eur. J. Inorg. Chem.* 2008 (2008) 2177–2185.
- [45] H. Dinçalp, Ş. Kızılok, S. İcli, *Dyes Pigm.* 86 (2010) 32–41.
- [46] J.R. Knutson, J.M. Beechem, L. Brand, *Chem. Phys. Lett.* 102 (1983) 501–507.
- [47] J.C. Scaiano, *CRC Handbook of Organic Photochemistry*, Taylor & Francis Group, 1989.
- [48] M. Maus, R. De, M. Lor, T. Weil, S. Mitra, U.M. Wiesler, A. Herrmann, J. Hofkens, T. Vosch, K. Mullen, F.C. De Schryver, *J. Am. Chem. Soc.* 123 (2001) 7668–7676.
- [49] J. Pommerehne, H. Vestweber, W. Guss, R.F. Mahrt, H. Bassler, M. Porsch, J. Daub, *Adv. Mater.* 7 (1995) 551–554.
- [50] M.H. Kim, M.J. Cho, K.H. Kim, M.H. Hoang, T.W. Lee, J.-I. Jin, N.S. Kang, J.-W. Yu, D.H. Choi, *Org. Electron.* 10 (2009) 1429–1441.
- [51] B.R. Sim, B.G. Kim, J.K. Lee, J.Y. Do, *Thin Solid Films* 519 (2011) 8091–8094.
- [52] N.I. Craciun, J. Wildeman, P.W.M. Blom, *Phys. Rev. Lett.* 100 (2008) 056601–056605.
- [53] M.M. Mandoc, L.J.A. Koster, P.W.M. Blom, *Appl. Phys. Lett.* 90 (2007) 133504:1–133504:3.
- [54] P.W.M. Blom, M.J.M. de Jong, M.G. van Munster, *Phys. Rev. B* 55 (1997) R656–R659.
- [55] J.-H. Kim, H.U. Kim, D. Mi, S.-H. Jin, W.S. Shin, S.C. Yoon, I.-N. Kang, D.-H. Hwang, *Macromol.* 45 (2012) 2367–2376.